Thermal Stability, Crystallization Behavior, and Phase Morphology of Poly(ε-caprolactone)diol-*grafted*-Multiwalled Carbon Nanotubes

R. N. Jana,[1] Jae Whan Cho[2]

[1]*Artificial Muscle Research Center, Konkuk University, Seoul 143-701, Korea*
[2]*Department of Textile Engineering, Konkuk University, Seoul 143-701, Korea*

Received 11 March 2008; accepted 15 May 2008
DOI 10.1002/app.28710
Published online 23 July 2008 in Wiley InterScience (www.interscience.wiley.com).

ABSTRACT: Poly(ε-caprolactone)diol (PCL) with five different molecular weights (e.g., 400, 2000, 3000, 4000, and 8000 g/mol) was grafted onto the surface of functionalized-multiwalled carbon nanotubes (f-MWNTs) by *grafting to* approach to form PCL-*grafted*-MWNTs (PCL-*g*-MWNTs). The grafting was confirmed by Fourier transform infrared spectroscopy and transmission electron microscopy (TEM). Thermal stability of PCL-*g*-MWNTs improved with the addition of f-MWNTs in PCL, and the maximum was observed at 6 wt % of f-MWNTs. Differential scanning calorimetric (DSC) studies showed that crystallization temperature, melting temperature, heat of crystallization, and heat of fusion decreased with the weight proportion of f-MWNTs in the composites, but they showed an increasing trend with increasing molecular weight of PCL in the composites. DSC results were of good agreement with the X-ray diffraction data, as crystallinity decreased with the incorporation of f-MWNTs in PCL. The crystallite size (P_{hkl}) of PCL in (110) direction increased, but in (200) direction it decreased. The size anisotropy (P_{110}/P_{200}) of the crystals in (110) and (200) directions increased regularly, indicating that the crystal growth was nonuniform in the two directions. The morphological observation by scanning electron microscopy and TEM showed that the PCL-*g*-MWNTs had higher diameter than raw multi-walled carbon nanotubes. Polarized optical microscopy showed that PCL-*g*-MWNTs had core/shell structure with the nanotubes as the 'hard' core and the hairy polymer layer as the 'soft' shell. © 2008 Wiley Periodicals, Inc. J Appl Polym Sci 110: 1550–1558, 2008

Key words: multiwalled carbon nanotubes; poly(ε-caprolactone); grafting; thermogravimetric analysis; scanning electron microscopy

INTRODUCTION

The discovery of multi-walled carbon nanotubes (MWNTs) in 1991 by Iijima[1] has opened a new era in the field of nanotechnology because of the excellent reinforcing and electrical properties of the MWNTs, arising from their special atomic and electronic structures. Nowadays, MWNTs have many important applications, which include catalysts support,[2–4] hydrogen storage,[5,6] reinforced materials,[7,8] nanoelectric devices,[9,10] field emission,[11,12] etc. However, their poor solubility and tendency to aggregate together limits their applications.[13–15] Thus, the composites prepared with unmodified MWNTs by means of mechanical dispersion show a limited improvement in tensile strength and modulus, because the reinforcement is achieved through adhesion and weak van der Waals forces, which gives rise to lower stress transfer ability. To have a higher stress transfer, a strong bonding between the MWNTs and polymer chains is necessary. Several approaches including sidewall functionalization,[16–18] polymer encapsulation,[19,20] and polymer grafting[21] have been tried to overcome these problems. Among these approaches, polymer grafting may be more effective due to its strong chemical bonding between polymer and MWNTs. The so-called *grafting to* approach where macromolecules with terminal functional groups are attached to the surface of MWNTs, and *grafting from* approach where *in situ* polymerization of monomers in the presence of MWNTs or MWNTs-based macroinitiators are employed to make the MWNTs-polymer composites. Till date, various polymers such as polystyrene,[21] polymethylmethacrylate,[22] polyimide,[23] and polyvinyl alcohol[24] have been successfully grafted onto MWNTs surfaces by the *grafting to* or *grafting from* approach. The grafted MWNTs have shown many examples of a good solubility or dispersibility in different solvents and polymer matrix.

Poly(ε-caprolactone)diol (PCL) may react with diisocyanate to give polyurethane elastomer. As it acts

Correspondence to: J. W. Cho (jwcho@konkuk.ac.kr).
Contract grant sponsor: Korea Research Foundation Grant; contract grant number: KRF-2004-005-B00046.
Contract grant sponsor: MOST/KOSEF (SRC/ERC program); contract grant number: R11-2005-065.

TABLE I
Composition for PCL-*g*-MWNTs

Sample code	MW of PCL					f-MWNTs (wt %)
	3000 (wt %)	400 (wt %)	2000 (wt %)	4000 (wt %)	8000 (wt %)	
P-100	100	0	0	0	0	0
P-302	100	0	0	0	0	2
P-305	100	0	0	0	0	5
P-306	100	0	0	0	0	6
P-307	100	0	0	0	0	7
P-310	100	0	0	0	0	10
P-400	0	100	0	0	0	6
P-206	0	0	100	0	0	6
P-406	0	0	0	100	0	6
P-806	0	0	0	0	100	6

as a soft segment in polyurethane chain, the different molecular weight of PCL may impart different flexibility to the polyurethane chain. Moreover, polyurethane/MWNTs composites are also recognized as the composites for artificial muscle, which may find application in biomedical applications like microsurgical devices, artificial limbs, or even implants of muscles in hearts.[25] Again the dispersion of MWNTs in PU matrix is still not so good due to weak interfacial interaction with the polymer matrix.[26–28] That problem may be solved by grafting of PCL onto the surface of MWNTs and then by the reaction of the grafted MWNTs with diisocyanate to get PU/MWNTs composite.

In this study, the grafting of PCL with five different molecular weights has been done onto the surface of functionalized-multiwalled carbon nanotubes (f-MWNTs) by *grafting to* approach, and thermal stability, crystallization behavior, and phase morphology of PCL-*grafted*-MWNTs (PCL-*g*-MWNTs) are investigated.

EXPERIMENTAL

Materials

MWNTs of grade CM-95 was supplied by Iljin Nanotech Co., Seoul, Korea, with an average diameter of 10–15 nm, length 10–20 μm, and a purity of 95%. PCL of different molecular weight of 400, 2000, 3000, 4000, and 8000 g/mol was received from Solvay Co., Cheshire, UK. Thionyl chloride, nitric acid, and sulfuric acid were of laboratory grade reagents.

Preparation of PCL-*g*-MWNTs

Typically, 2.0 g of MWNTs, 20 mL of 60% HNO_3, and 60 mL of 98% H_2SO_4 were added into 500-mL flask equipped with a condenser with vigorous stirring. The flask was then immersed in a sonication bath using a high power ultrasonic processor for 10 min. The mixture was then stirred for 100 min under reflux (100–130°C). During this period, dense brown gas was collected and treated with a NaOH aqueous solution connected to the condenser. After cooling to room temperature, the reaction mixture was diluted with 100 mL distilled water and then vacuum filtered through a filter paper (Minipore 1.0 μm). The solid was dispersed in 100 mL of water and filtered again. The dispersion, filtering, and washing steps were continued until the pH of the residue reached to seven. The filtered solid was then washed with 50 mL of acetone to remove most of the water from the sample. Then the solid was dried under vacuum at 60°C for 24 h.

About 20 mL of thionyl chloride ($SOCl_2$) with 1.0 g of carboxylated MWNTs was taken in a flask, and reflux was continued for 24 h at 65°C. The residual $SOCl_2$ was removed by reduced pressure distillation and then the as-produced acylchloride-functionalized MWNTs (f-MWNTs) was reacted with required quantity of different MW of PCL at 65°C for 24 h (Table I) to get PCL-*g*-MWNTs. To eliminate the unreacted PCL, the resulting reaction product was dissolved in excess of chloroform ($CHCl_3$) and vacuum filtered through a membrane (Minipore 1.0 μm). The samples are coded as P-302, P-305, P-306 etc, where the first digit indicates the MW of PCL in thousand, whereas the last digit indicates the wt % of MWNTs in the composites. However, P-100 indicates the neat PCL of MW 3000, and P-400 indicates PCL-*g*-MWNTs containing 6 wt % of MWNTs in PCL of MW 400, respectively, (Table I).

Characterization

Fourier transform infrared (FTIR) spectroscopic measurements were performed using a Jasco FTIR 300E with an attenuated total reflectance method.

Thermogravimetric (TG) and derivative thermogravimetric (DTG) analyses of the composites and

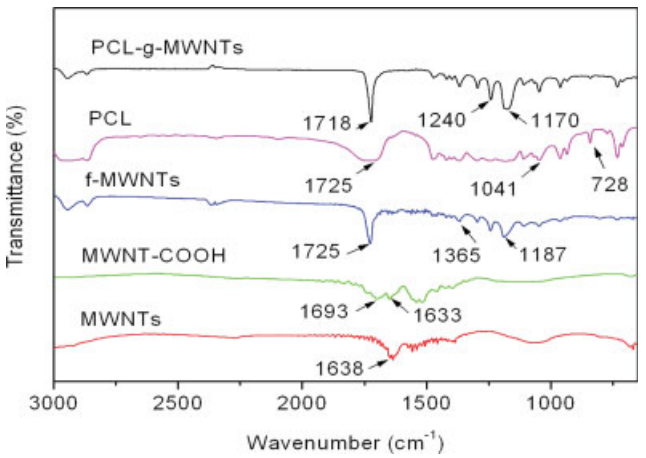

Figure 1 FTIR spectra of raw MWNT, MWNT-COOH, f-MWNT, and PCL-*g*-MWNTs. [Color figure can be viewed in the online issue, which is available at www.interscience.wiley.com.]

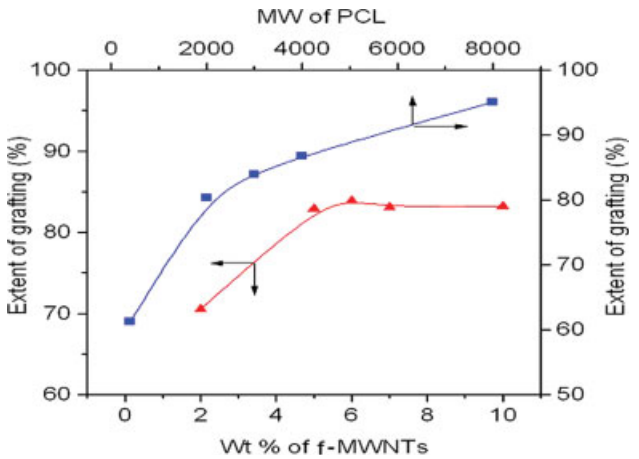

Figure 3 Extent of grafting with wt % of PCL (MW = 3000) and MW of PCL in the samples. [Color figure can be viewed in the online issue, which is available at www.interscience.wiley.com.]

pure components were carried out in a thermogravimetric analyzer (TGA Q2050) equipped with a computer data analyzer. The studies were done from

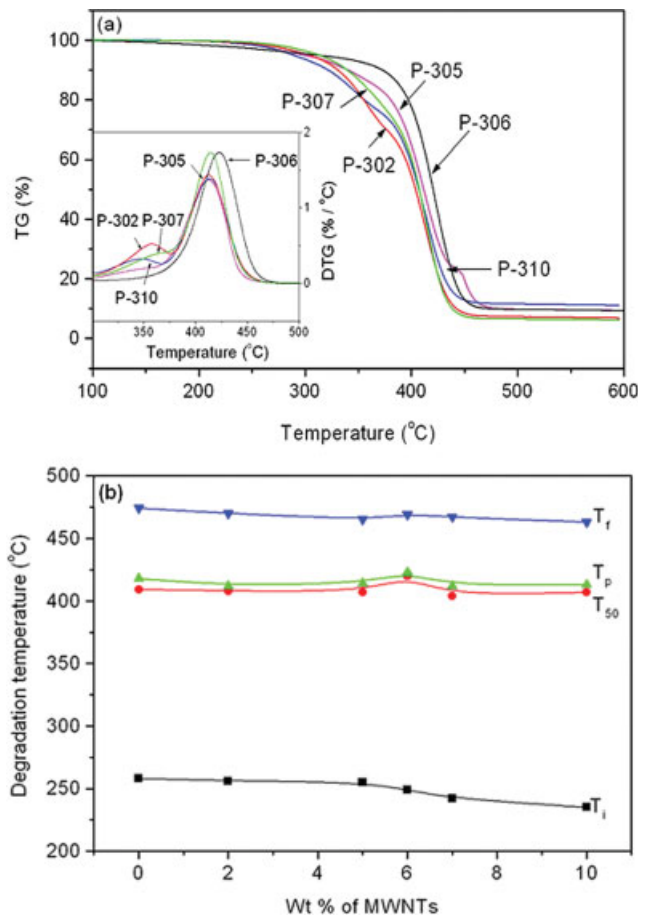

Figure 2 Thermogravimetric analysis of PCL-*g*-MWNTs (a) TG and DTG curves of samples containing different wt % of PCL (MW = 3000) and (b) variation of degradation temperatures with wt % of MWNTs in the composites. [Color figure can be viewed in the online issue, which is available at www.interscience.wiley.com.]

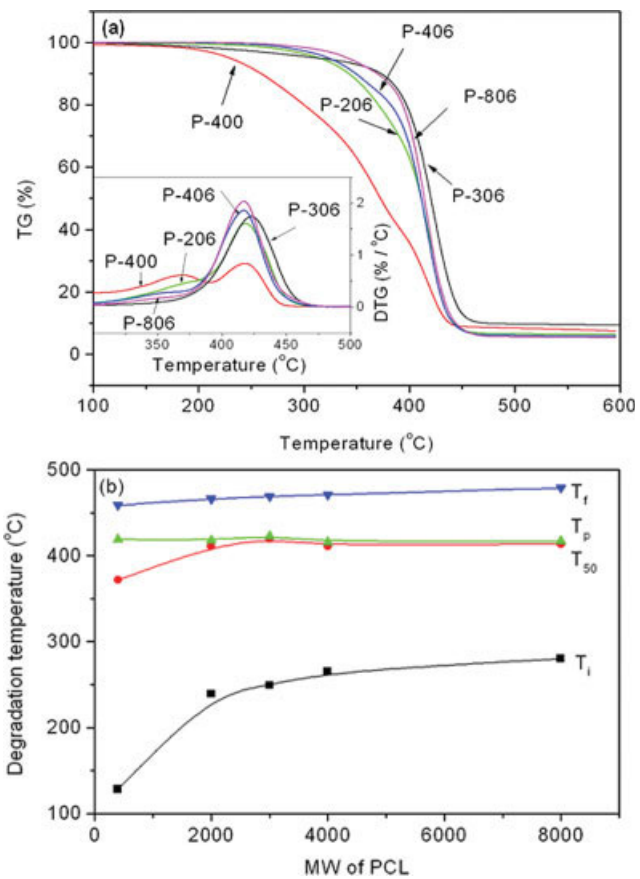

Figure 4 Thermogravimetric analysis of PCL-*g*-MWNTs (a) TG and DTG curves of composites containing the different MW of PCL and (b) variation of degradation temperatures with MW of PCL. [Color figure can be viewed in the online issue, which is available at www.interscience.wiley.com.]

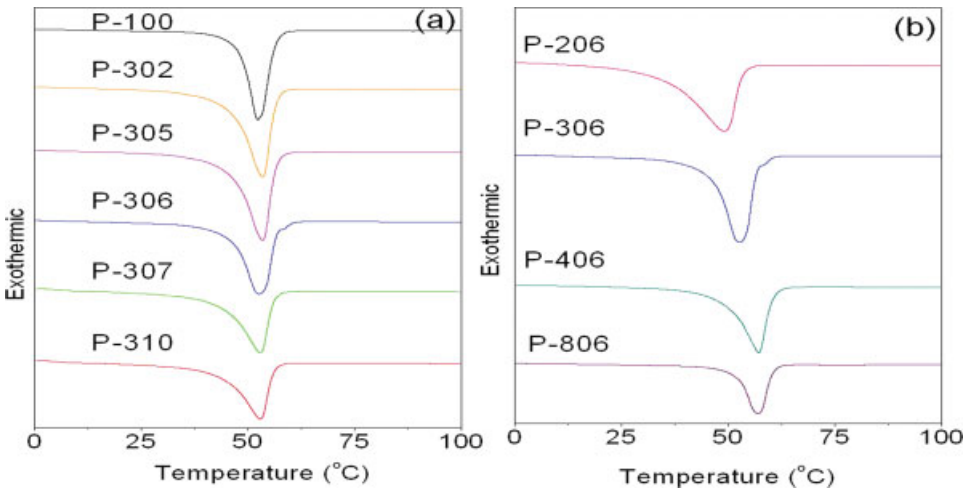

Figure 5 DSC curves of samples obtained during heating. [Color figure can be viewed in the online issue, which is available at www.interscience.wiley.com.]

room temperature to 600°C (except for MWNTs) under nitrogen atmosphere at a flow rate of 50 mL/min and a heating rate of 10°C/min.

The extent of PCL grafting[29] was calculated according to eq. (1) from the TG data assuming that the residue left at 480°C after thermal degradation was the weight of MWNTs only. Thus, the difference between the initial weight of the sample taken for TG study and the residue left after the study would give rise to the weight of the grafted PCL in that composite. Moreover, based on the residue left, the total amount of PCL, which was taken for the sample preparation, can be calculated back.

$$\text{Extent of grafting}\,(\%) = (W_o - W_f)/W_c \qquad (1)$$

where W_o is the initial weight of the sample taken for TG study, W_f is the weight of the residue left, and W_c is the weight of the PCL taken for grafting reaction with MWNTs.

Differential scanning calorimetric (DSC) measurements were carried out using a TA instrument 2010 thermal analyzer in the temperature range of 0–100°C under nitrogen atmosphere at a flow rate of 50 mL/min. During the first and second heating the rate of heating was 10°C/min in both the cases, but the rate of cooling was 2°C/min. The peak crystallization temperature (T_c) and heat of the crystallization (ΔH_c) were obtained during cooling of the melt after first heating, whereas the melting temperature (T_m) and the endothermic heat of fusion (ΔH_f) were obtained during the second heating of the samples.

Wide angle X-ray diffraction measurements using Cu Kα radiation and a nickel filter were carried out in a diffractometer (Bruker AXS, X-ray diffractometer). The diffraction was recorded in the angular range of $2\theta = 10$–40° at a scanning speed 5°/min.

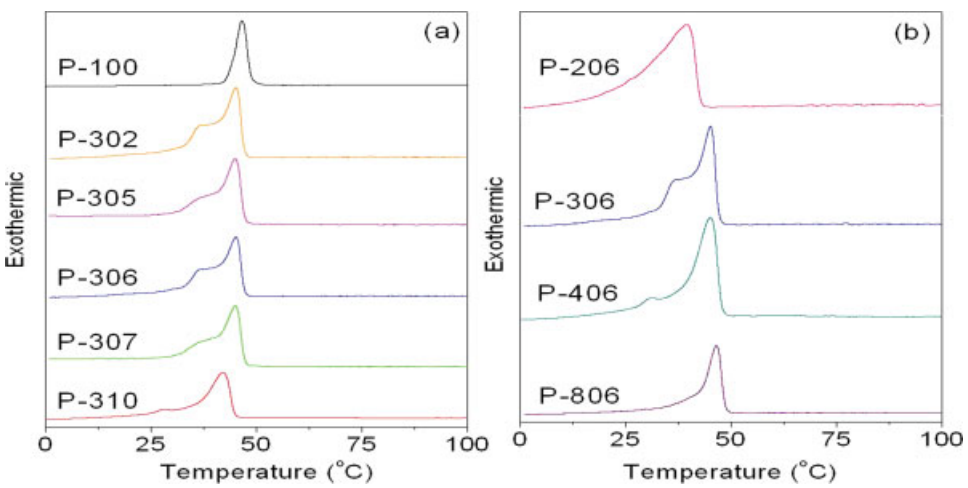

Figure 6 DSC curves of samples obtained during cooling from the melts. [Color figure can be viewed in the online issue, which is available at www.interscience.wiley.com.]

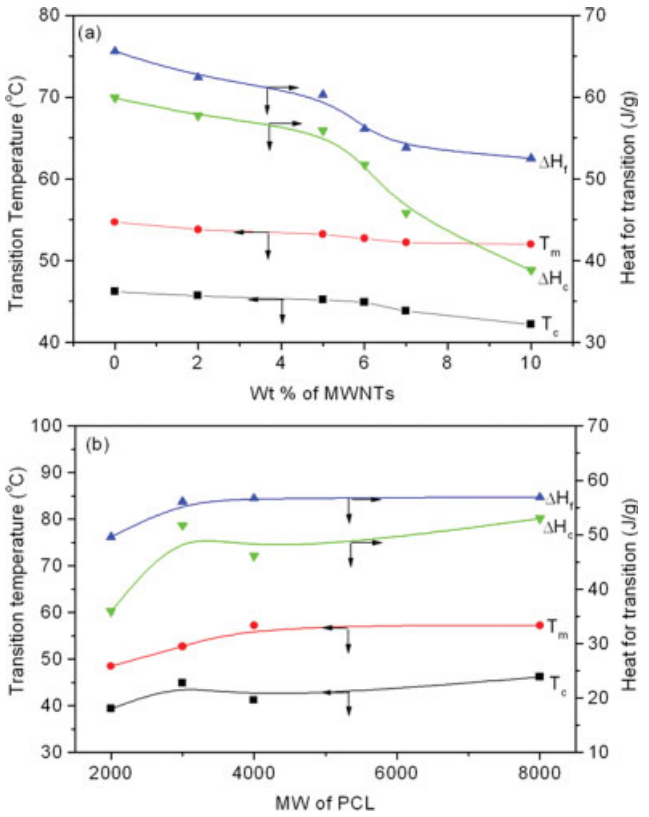

Figure 7 Variation of transition temperature and heat for transition with (a) wt % of MWNTs and (b) MW of PCL. [Color figure can be viewed in the online issue, which is available at www.interscience.wiley.com.]

The area ratio of crystalline peaks to the total area of crystalline and amorphous peaks was used as the measure of crystallinity. The crystallite size (P_{hkl}) and interchain distance (r_{hkl}) were calculated from Scherrer equation,[30]

$$P_{hkl} = K\lambda/\beta \cos\theta \quad (2)$$

$$r_{hkl} = \lambda/2 \sin\theta \quad (3)$$

where K is a Scherrer constant which equals to 0.9, λ is the wavelength of the radiation (1.54 Å for Cu Kα), β is the width of the peak at half maximum, and θ is the angle of incidence.

Morphology of the samples was observed under a scanning electron microscope (SEM) (Hitachi *S*-4200) after sputter coated with gold to facilitate scanning under SEM at a 0° tilt angle. Morphological analysis of the samples was also carried out by transmission electron microscopy (TEM). Samples for TEM were prepared by dispersing the sample in ether and then placing a drop of suspension on one side of the transparent polymer coated 200 mesh copper grid. TEM images were taken with a ZEISS LIBRA®-120, the energy filtering TEM combine with state of the art electron optics with unique Koehler illumination. Polarized optical microscope (Eclipse LV 100 POL) from Nikon Corp., Tokyo, Japan, equipped with a hot stage (LTS 350) from Linkon Scientific Instruments Ltd, England, UK, was used.

RESULTS AND DISCUSSION

Grafting of PCL and MWNTS

FTIR spectra of unmodified MWNTs show a peak with very low intensity at 1638 cm^{-1}, corresponding to C=O stretching[31] (Fig. 1). After the oxidation with the mixture of the acids, C=O stretching is shifted to 1693 cm^{-1} and 1633 cm^{-1}. These peaks are assigned for free carbonyl groups and hydrogen bonded carbonyl groups of the MWNTs, respectively.[31] Acylation of carboxylic groups leads to a formation of carbonyl peak at 1725 cm^{-1} and new

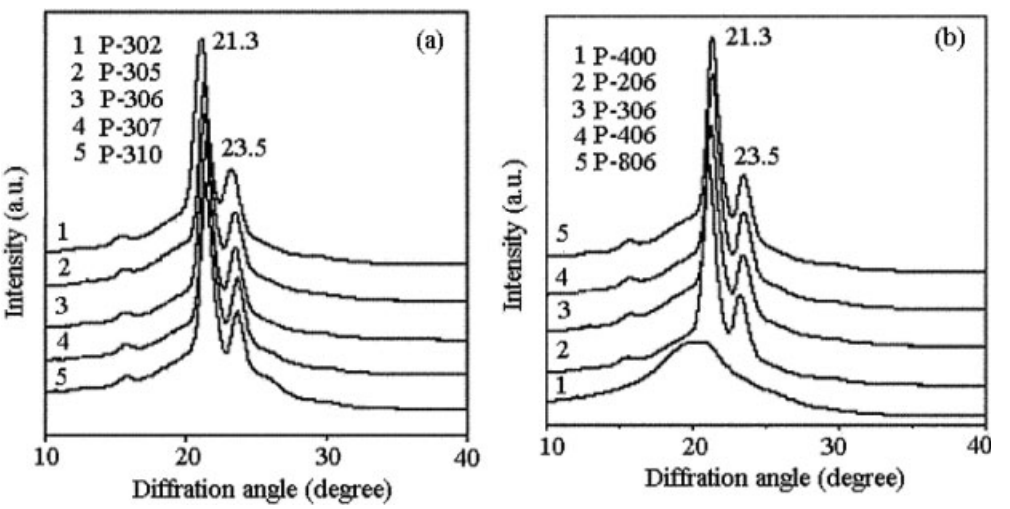

Figure 8 X-ray diffractograms for PCL-*g*-MWNTs (a) with varying wt % of f-MWNTs at the constant MW of 3000 g/mol and (b) with varying MW of PCL at the constant wt % of f-MWNTs.

TABLE II
Degree of Crystallinity (X_c), Crystallite Sizes (P_{110}, P_{200}), Size Anisotropy (P_{110}/P_{200}), and Inter-Chain Distances (r_{110}, r_{200}) of PCL and PCL-*g*-MWNTs

Samples code	P_{110} (Å)	P_{200} (Å)	P_{110}/P_{200}	r_{110} (Å)	r_{200} (Å)	X_c (%)
P-100	64.7	64.9	0.99	4.18	3.78	38.8
P-302	18.3	7.9	2.31	4.26	3.91	37.9
P-305	16.8	8.0	2.10	4.21	3.83	37.1
P-306	15.3	8.7	1.75	4.17	3.78	37.0
P-307	15.2	9.5	1.60	4.16	3.78	36.9
P-310	12.1	10.1	1.19	4.15	3.76	35.7
P-400	–	–	–	–	–	–
P-206	10.1	9.5	1.06	4.22	3.82	35.2
P-406	10.8	8.9	1.21	4.16	3.78	36.3
P-806	15.2	8.7	1.74	4.16	3.78	37.3

peaks at 1365 cm^{-1} and 1187 cm^{-1}. The new peaks appeared may be due to C—Cl bond formation. Neat PCL have a broad C=O stretching at 1725 cm^{-1} and C—O stretching at 1041 cm^{-1}. After reaction with PCL along with the carbonyl peak, two new peaks at 1240 cm^{-1} and 1170 cm^{-1} have been appeared. The peaks at 1240 cm^{-1} and 1170 cm^{-1} may be due to the formation C—O bond by the reaction between acylchloride groups (—COCl) of f-MWNTs and hydroxyl groups (—OH) of PCL. As a result, it can be seen that there is a covalent bond formation between PCL and f-MWNTs.

Thermal stability of PCL-*g*-MWNTs

The different degradation temperatures obtained from TG and DTG curves of PCL-*g*-MWNTs with different weight proportion of f-MWNTs as shown in Figure 2(a) are plotted in Figure 2(b). The temperature of initial degradation (T_i), which is defined as temperature at which 1% of the material has been degraded, decreases regularly with the increase in wt % of f-MWNTs in the composites. The decrease in T_i values is due to the increased proportion of the carbonyl groups coming from the f-MWNTs. The carbon atoms of the f-MWNTs attached to the carboxylic group are sp^3 hybridized. This causes high inherent strain, which makes them more susceptible to thermal degradation. The peak temperature (T_p), where the degradation rate becomes the maximum, for the samples with different wt % of MWNTs is almost same (412–414°C) except for P-306 (423°C). P-306 also has the highest T_{50}, defined as temperature at which 50% of the material has been degraded, and T_f, defined as temperature of finish. But when the proportion of f-MWNTs in the composite is further increased (> 6%), the T_p value reduces. The highest thermal stability of P-306 is due to the optimum interaction of PCL with f-MWNTs at this level. At higher wt % (> 6%) of f-MWNTs, there may not be any remaining reactive sites (—OH) of PCL, so the excess f-MWNTs will remain as unreacted. This is in agreement with the extent of grafting with the wt % of MWNTs in the composites. The extent of grafting increases initially with the amount of f-MWNTs in the composites, and then it becomes almost constant after 6 wt % of MWNTs as shown in Figure 3. As the amount of f-MWNTs increases in the composites, the extent of reaction between —OH group of PCL and —COCl group of f-MWNTs

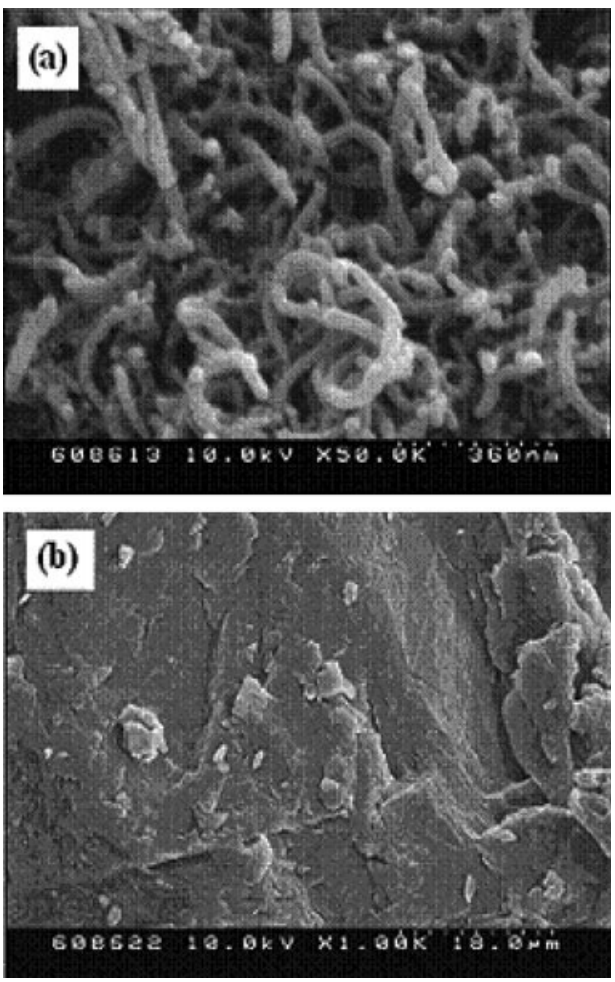

Figure 9 SEM photographs of (a) raw MWNTs and (b) PCL.

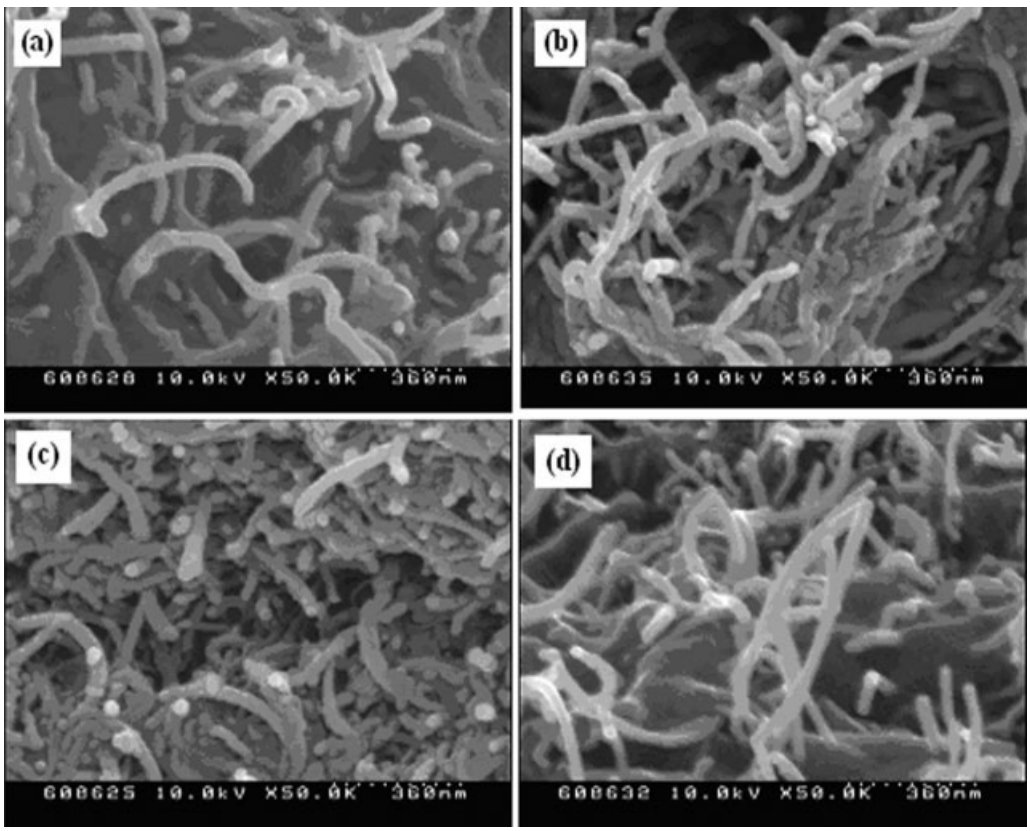

Figure 10 SEM photographs of (a) P-302, (b) P-305, (c) P-306, and (d) P-310.

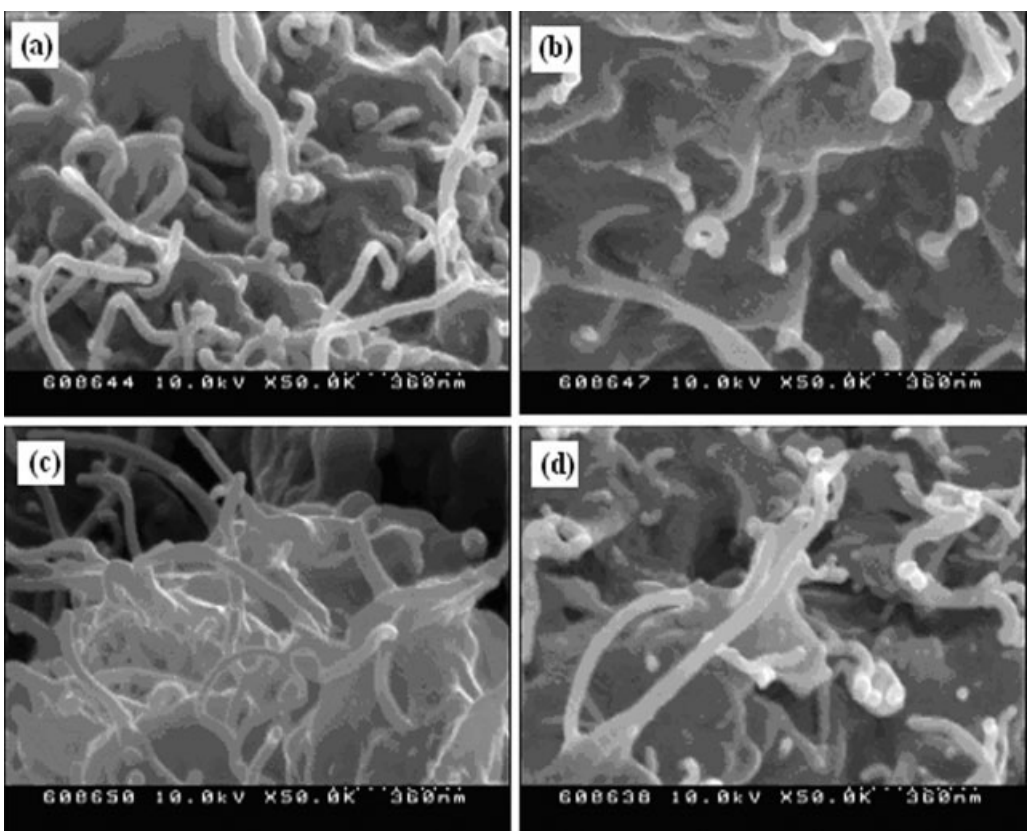

Figure 11 SEM photographs of (a) P-400, (b) P-206, (c) P-406, and (d) P-806.

increases up to 6 wt % of f-MWNTs, afterwards there is no such residual reactive functional group (—OH) of PCL for further reaction. But with the increasing molecular weight of PCL, there is a continuous increase in the extent of grafting. This may be due to the increase in the molecular chain length of the PCL molecules.

TG and DTG curves for PCL-*g*-MWNTs with different molecular weight of PCL are shown in Figure 4(a), and the different degradation temperatures as obtained from the curves are plotted in Figure 4(b). With the increase in the molecular weight of PCL, there is an increasing trend in T_i values. For instance, 128, 239, 249, 265 and 280°C are the T_i values for PCL with molecular weight of 400, 2000, 3000, 4000, and 8000 g/mol, respectively [Fig. 4(b)]. The increase in T_i values with the molecular weight of PCL is the characteristics initial degradation temperature of the PCL molecules. T_p for the composites with different molecular weight is almost same (except MW = 3000) in the range of 416–419°C. Their 50% degradation occurs at about 372–414°C, and the degradation completes within 459–479°C.

Crystallization of PCL-*g*-MWNTs

The DSC heating and cooling traces of different samples are shown in Figures 5 and 6, respectively. The crystallization and melting temperatures and heats of crystallization and fusion obtained from the DSC traces are plotted in Figure 7. T_m and T_c decrease with increase of f-MWNTs in the composites. This suggests that the crystalline phase in the composites is less perfect than that of pure PCL. This is due to the presence of more heterogeneous nucleation, which reduces the perfection of PCL crystallites in the composites.[32] Both ΔH_f and ΔH_c decrease with wt % of f-MWNTs, indicating that the crystallinity of the sample becomes lower. This result is in good agreement with the X-ray diffraction studies. The degree of crystallinity (X_c), crystallite sizes (P_{110}, P_{200}), size anisotropy (P_{110}/P_{200}), and interchain distances of the PCL-*g*-MWNTs, measured from the X-ray diffraction patterns (Fig. 8) for the samples are summarized in Table II. With the addition of f-MWNTs in the PCL, X_c decreases regularly. The peaks near $2\theta = 21.3$ and 23.5° are due to the presence of PCL crystals in samples, which correspond to (110) and (200) reflections, respectively.[32] Moreover, the crystallite size in (110) direction increases, but in (200) direction it decreases with an increase in f-MWNTs proportion in the composites. So the extent of folding of the PCL chains on the surface of the f-MWNTs in (110) direction is more favorable than (200) direction. As a result, the size anisotropy (P_{110}/P_{200}) of the crystals for all the samples increases regularly, indicating that the crystal growth is nonuniform in two directions. Consequently, the interchain distances (r_{110}, r_{200}) gradually increases with an increase in f-MWNTs in the samples. The X-ray diffraction pattern for the samples containing increasing molecular weight of PCL is shown in Figure 8(b). With increasing molecular weight of PCL, the increased degree of crystallinity of the samples is due to the higher percent of the crystallinity of the individual PCL molecules.

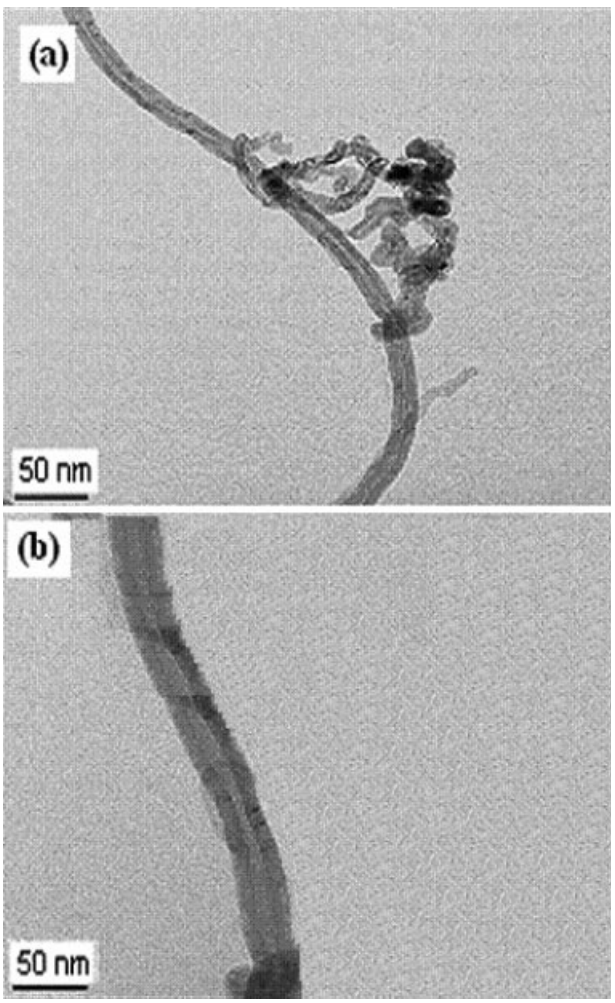

Figure 12 TEM photographs of (a) MWNTs and (b) PCL-*g*-MWNTs (P-306).

Phase morphology of PCL-*g*-MWNTs

Figure 9 shows the SEM micrographs for raw MWNTs and PCL. It is clear from the figure that the raw MWNTs have almost smooth tubular structure without any noticeable aggregation of the nanotubes as shown in Figure 9(a). Figure 9(b) shows a SEM micrograph with low magnification of 1000× for PCL flakes. It is clear from the micrograph that PCL has layer structure. Figure 10 shows the SEM photographs for the samples containing different weight proportion of f-MWNTs in the composites with PCL

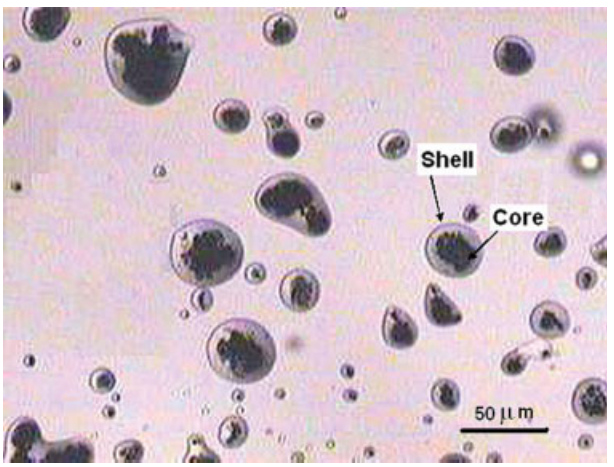

Figure 13 POM of PCL-*g*-MWNTs (P-306) at a magnification of ×200. [Color figure can be viewed in the online issue, which is available at www.interscience.wiley.com.]

of MW of 3000 g/mol. As the weight proportion of f-MWNTs increases in the samples, the amount of the grafted PCL increases which is clear from their increased diameter of MWNTs. The average diameter of MWNTs has been increased from 25 nm for P-302 to 35 nm for P-306 and P-310. Similarly, with the increasing MW of PCL, the diameter of the PCL-*g*-MWNTs also increases due to their higher chain length of the PCL molecules (Fig. 11).

The grafting has also been confirmed from their TEM studies. Figure 12 shows the TEM photographs of raw MWNTs and PCL-*g*-MWNTs. The raw MWNTs show almost smooth surface [Fig. 12(a)] as there is no such functional group on the surface. After grafting of PCL onto the surface of the f-MWNTs, the surface becomes very rough [Fig. 12(b)], and the diameter of the MWNTs has been increased by 10–15 nm, approximately. This is due to scaffolding of the PCL chain onto the surface of the MWNTs, which may be a direct evidence for grafting reaction of PCL. Polarized optical microscopy (POM) of PCL-*g*-MWNTs is found to have core/shell structure with the nanotubes as the hard core and the hairy polymer layer as the soft shell (Fig. 13).

CONCLUSIONS

PCL was covalently grafted onto the surface of f-MWNTs, which was confirmed by FTIR spectroscopy and TEM observation. Thermal stability of the composites was improved slightly with the addition of f-MWNTs in PCL and found to be the maximum at 6 wt % of f-MWNTs. The crystallization and melting temperatures and heats of crystallization and fusion decreased with the wt % of f-MWNTs in the composites. The crystallinity of the composites decreased with the incorporation of f-MWNTs in PCL. The morphological observation by SEM and TEM showed an increase in the diameter of MWNTs after grafting with PCL. POM showed that the composites had core/shell structure, where the nanotubes formed the hard core and the hairy polymer layer formed the soft shell.

References

1. Iijima, S. Nature 1991, 354, 56.
2. Garcia, J.; Gomesh, T.; Serp, P.; Kalck, P.; Figueiredo, J. L.; Faria, J. L. Catal Today 2005, 102, 101.
3. Yao, Y.; Ding, Y.; Ye, L. S.; Xia, X. H. Carbon 2006, 44, 61.
4. Serp, P.; Feurer, R.; Faria, J. L.; Figueiredo, J. L. J Phys IV (France) 2002, 12, 24.
5. Ning, G. Q.; Wei1, F.; Luo, G. H.; Wang, Q. X.; Wu, Y. L.; Yu, H. Appl Phys A 2004, 78, 955.
6. Gundiah, G.; Govindaraj, A.; Rajalakshmi, N.; Dhathathreyan, K. S.; Rao, C. N. R. J Mater Chem 2003, 13, 209.
7. Kireitseu, M. Adv Sci Technol 2006, 50, 31.
8. Sulong, A. B.; Park, J.; Lee, N.; Goak, J. J Compos Mater 1947 2006, 40.
9. Jun, S. C.; Choi, J. H.; Cha, S. N.; Baik, C. W.; Lee, S.; Kim, H. J.; Hone, J.; Kim, J. M. Nanotechnology 2007, 18, 255701.
10. Wang, X.; Lu, G.; Lu, Y. J. Int J Solids Struct 2007, 44, 336.
11. Lyth, S. M.; Oyeleye, F.; Curry, R. J.; Davis, J.; Silva, S. R. P. J Vac Sci Technol B 2006, 24, 1362.
12. Saito, Y.; Hamaguchi, K.; Uemura, S.; Uchida, K.; Tasaka, Y.; Ikazaki, F.; Yumura, M.; Kasuya, A.; Nishina, Y. Appl Phys A 1998, 67, 95.
13. Georgakilas, V.; Kordatos, K.; Prato, M.; Guldi, D. M.; Holzinger, M.; Hirsch, A. J Am Chem Soc 2002, 124, 760.
14. Shim, M.; Kam, N. W. S.; Chen, R. J.; Li, Y. M.; Dai, H. J. Nano Lett 2002, 2, 285.
15. Garg, A.; Sinnott, S. B. Chem Phys Lett 1998, 295, 273.
16. Zhang, L.; Kiny, V. U.; Peng, H. Q.; Zhu, J.; Lobo, R. F. M.; Margrav, J. L.; Khabashesku, V. N. Chem Mater 2004, 16, 2055.
17. Holzinger, M.; Vostrowsky, O.; Hirsch, A.; Hennrich, F.; Kappes, M.; Weiss, R.; Jellen, F. Angew Chem Int Ed 2001, 40, 4002.
18. Seifert, G.; Kohler, T.; Frauenheim, T. Appl Phys Lett 2000, 77, 1313.
19. Tang, B. Z.; Xu, X. Macromolecules 1999, 32, 2569.
20. Xia, H. S.; Wang, Q.; Qiu, G. H. Chem Mater 2003, 15, 3879.
21. Andrews, R.; Jacques, D.; Minot, M.; Rantell, T. Macromol Mater Eng 2002, 287, 395.
22. Kong, H.; Gao, C.; Yan, D. Y. J Am Chem Soc 2004, 126, 412.
23. Hu, N.; Zhou, H.; Dang, G.; Rao, X.; Chen, C.; Zhang, W. Polym Int 2007, 56, 655.
24. Naebe, M.; Lin, T.; Tian, W.; Dai, L.; Wang, X. Nanotechnology 2007, 18, 225605.
25. Santerre, J. P.; Woodhouse, K.; Laroche, G.; Labow, R. S. Biomaterials 2005, 26, 7457.
26. Lee, C. H.; Liu, J. Y.; Chen, S. L.; Wang, Y. Z. Polym J 2007, 39, 138.
27. Bliznyuk, V.; Singamaneni, S.; Kattumenu, R. Appl Phys Lett 2006, 88, 164101.
28. Paik, I. H.; Goo, N. S.; Jung, Y. C.; Cho, J. W. Smart Mater Struct 2006, 15, 1476.
29. Lou, X.; Detrembleur, C.; Sciannamea, V.; Pagnoulle, C.; Jerome, R. Polymer 2004, 45, 6097.
30. Alexander, L. E. X-ray Diffraction Methods in Polymer Science; Wiley Interscience: New York, 1969.
31. Sahoo, N. G.; Jung, Y. C.; Yoo, H. J.; Cho, J. W. Macromol Chem Phys 2006, 207, 1773.
32. Wu, T. M.; Chen, E. J Polym Sci Part B: Polym Phys 2006, 44, 598.